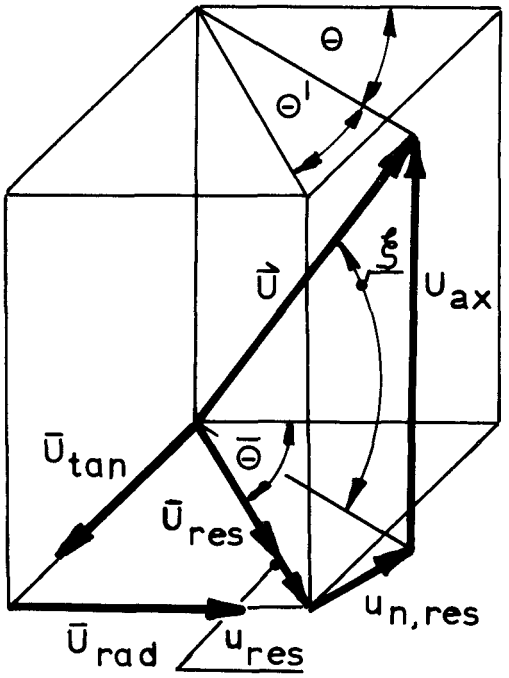

Fig. A2. Velocities and angles used for calculating of the energy flux through control surface 1.

tropic at any z in the impeller stream at $s = 7$ cm:

$$\overline{u^2_{n,\mathrm{res}}} = \overline{u^2_{\mathrm{ax}}} = \overline{u^2_{\mathrm{res}}} \qquad \text{(A15)}$$

Incorporating these simplifications and neglecting fluctuating velocities raised to the power 3, we get

$$I_1 = \pi r_1 \rho \int_{-z_2}^{z_2} [(\overline{U^3_{\mathrm{res}}} + 5\overline{U}_{\mathrm{res}}\,\overline{u^2_{\mathrm{res}}}) \cos\overline{\theta} - 2\overline{U}_{\mathrm{res}}\,\overline{u^2_{\mathrm{res}}} \sin\overline{\theta}]\, dz \qquad \text{(A16)}$$

The flux of kinetic energy through control surface 2 was determined similarly by assuming that $\overline{U}_{\mathrm{rad}}$ was negligible and that the flow was isotropic:

$$I_2 = 2\pi\rho \int_0^{r_1} [(\overline{U^3}_{\mathrm{res},at} + 5\overline{U}_{\mathrm{res},at}\,\overline{u^2}_{\mathrm{res},at}) \cos\overline{\zeta} - 2\overline{U}_{\mathrm{res},at}\,\overline{u^2}_{\mathrm{res},at} \sin\overline{\zeta}]\, r dr \qquad \text{(A17)}$$

$\overline{U}_{\mathrm{res},at}$ is the sum of the velocity components $\overline{U}_{\mathrm{ax}}$ and $\overline{U}_{\mathrm{tan}}$, and $u_{\mathrm{res},at}$ is the fluctuating velocity in direction of $\overline{U}_{\mathrm{res},at}$. The angles and velocity components are shown in Figure A3.

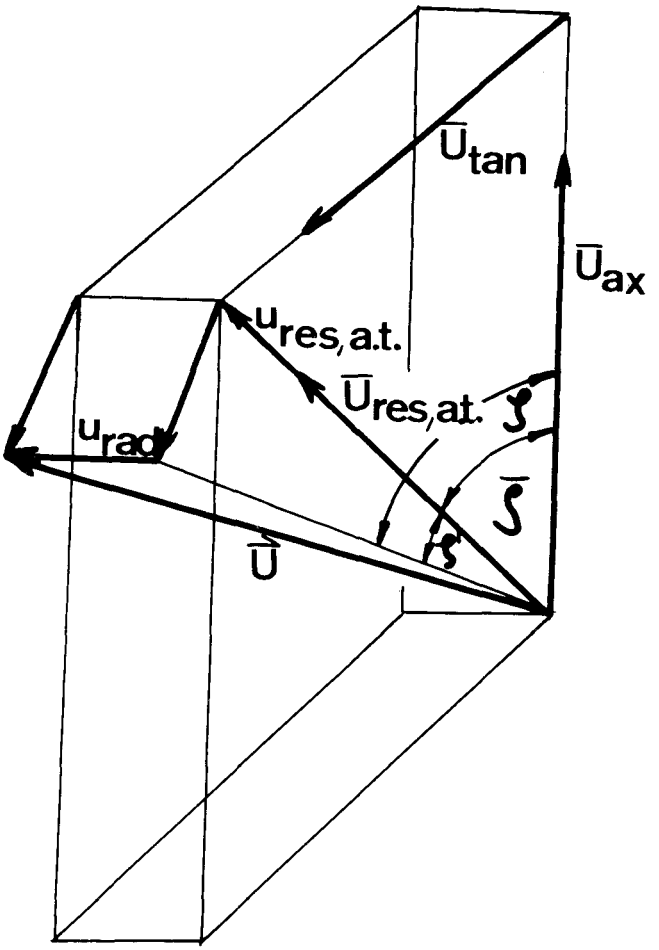

Fig. A3. Velocities and angles used for calculating the energy flux through control surface 2.

All the terms in Equations (A16) and (A17) were obtained from measured velocities. The control surfaces were set at $s = 7$ cm and $z_2 = \pm 3.75$ cm for the data presented in Table 2.

Manuscript received June 10, 1974; revision received and accepted April 30, 1975.

Part II. The Bulk of the Tank

Turbulence parameters were measured in the bulk of turbulent stirred tanks of 45.7 and 91.4 cm diameter with air as the working fluid. Three types of turbine impellers were studied ranging in diameter from 22.8 to 45.7 cm. The turbulence in the bulk of the tank was essentially homogeneous and isotropic. The normalized one-dimensional energy spectra and the Eulerian autocorrelation functions were approximately the same throughout the tank and for all tanks, impellers, and operating conditions. The space averaged turbulent velocities were correlated by using the turbulent energy equation. A transformation of the measured spectra from the frequency space to the wave number space was accomplished. Integration of the dissipation spectra in the wave number space confirmed that most of the energy input is dissipated in the bulk of the tank through the turbulent motion. The results were extended to low viscosity liquid systems and used to interpret the data on mass transfer from suspended particles.

SCOPE

Constant power input per unit mass is a frequently used scale-up rule for turbulent stirred tanks (Uhl and Gray, 1966). The idea behind this rule is the intuitive assumption that equal power input per unit mass will lead to a similar intensity of fluid motion which in turn will lead to similar bulk mixing and turbulent mixing.

In Part I of this study it was shown that most of the power transmitted into a turbulent stirred tank is dissipated outside the impeller stream. It was also confirmed that the mean velocities and the velocity gradients are much smaller outside the impeller stream than inside. A consequence of these results is the conclusion that most of the energy transmitted into a turbulent stirred tank is dissipated through the turbulent motion. The objectives of this part of the study were to measure turbulence parameters in the bulk of a stirred tank, to relate these parameters to the power input, and to extend the results to liquid systems.

Two tanks were studied, one of 45.7 cm diameter and a second of 91.4 cm diameter. Three different types of turbine impellers were employed ranging in diameter from 22.8 to 45.7 cm. The power input per unit mass was varied by more than order of magnitude. The turbulence parameters were measured by using the shielded hot-wire of Gunkel et al. (1971).

CONCLUSIONS AND SIGNIFICANCE

The turbulence in the bulk of the tank was found to be approximately homogeneous and isotropic with the turbulent velocity having a variation about the space average value of the order of 15%. The normalized one-dimensional energy spectra were essentially the same everywhere in the tank and for all operating conditions. The spectra had a slope of about $-5/3$ in the low frequency range and a slope of about -7 in the high frequency range. The Eulerian autocorrelation functions were about the same for all operating conditions. The integral length scale of turbulence did not change significantly over the entire range of conditions. The most important conclusion in this part of the study was that the turbulence parameters are not directly related to the tank-impeller geometry but indirectly through the power input per unit mass.

The space average turbulent velocity was related to the power input per unit mass by using the turbulent energy equation. A semiempirical correlation obtained from wind tunnel studies was found to apply to the turbulence in the bulk of a stirred tank as well. The proposed correlations were extended to cover the more practical case of low-viscosity liquids.

A transformation of the spectra measured in the frequency space to the wave number space was accomplished without the use of Taylor's hypothesis. Integration of the dissipation spectra gave an independent measure of the energy dissipated in the bulk of the tank. It checked well with that obtained from the power correlations.

Inserting the turbulence parameters measured in this study into a form of the Frössling equation led to an equation having a form which was in agreement with experimental correlations relating the mass transfer from suspended particles to the power input per unit mass or to tank and impeller variables.

PREVIOUS WORK

In the two studies of the turbulence phenomena in stirred tanks reported to date, the streak lines of suspended particles were photographed. This method allows only the study of the large-scale, low-frequency features of the turbulence. Schwartzberg and Treybal (1968) found the following correlation between the root-mean-square turbulent velocity, the impeller speed, and the geometry of the system:

$$u' = 0.73\, ND[D/(T^2H)]^{1/3} \qquad (1)$$

The study of Levins and Glastonbury (1972) was limited to two pitched-blade impellers and two impeller speeds. Using a modified photographic technique which allowed them to distinguish the flow direction, they found turbulence intensities of about 75%. These values were about twice as large as those measured by Schwartzberg and Treybal (1968).

APPARATUS AND EXPERIMENTAL TECHNIQUE

The shielded hot-wire probe employed in Part I was used here. In addition to the standard tank (45.7 cm diameter) and impeller (22.8 cm impeller) described earlier, a second geometrically similar tank of 91.4 cm diameter and two other impellers were used. The dimensions of the impellers are given in Table 1. The right-hand column of the table gives the power numbers for these impellers. The power numbers for two of the impellers were given in the literature, while the third was estimated as follows. It was assumed that doubling the blade width of a disk style turbine would double the power number. This rule was shown to hold approximately for an open six-blade turbine by O'Connell and Mack (1950) and by Bates et al. (1963).

Axial, radial, and tangential fluctuating velocities were measured at a large number of locations in the bulk of the tank. In reporting much of the data, volume averaged values of the root-mean-square fluctuating velocity were used. These were obtained from

Table 1. Geometry of the Impellers

Impeller type	w/D	l/D	N_p	Reference
Six blade Disk style Turbine Impeller	0.2	0.25	5.0	Bates et al. (1963)
	0.4	0.25	10.0	Estimate
Four blade Turbine Impeller (No disk)	0.2	0.5	3.25	Bates et al. (1963)

Table 2. The Root-Mean-Square Velocities in the Standard System

$T = 45.7$ cm, $D = 22.8$ cm, $w/D = 0.2$, $l/D = 0.25$

N, s^{-1}	$\langle u'_{rad} \rangle$ m/s	$\frac{100\, s_v}{\langle u'_{rad} \rangle}$ %	$\langle u'_{tan} \rangle$ m/s	$\frac{100\, s_v}{\langle u'_{tan} \rangle}$ %	$\langle u'_{ax} \rangle$ m/s	$\frac{100\, s_v}{\langle u'_{ax} \rangle}$ %
6.67	0.31	26	0.40	38	0.50	22
10.0	0.54	22	0.70	27	0.90	14
13.3	0.79	22	0.91	17	1.22	16
15.8	0.96	21	1.16	22	1.53	14

$$\langle u' \rangle = \frac{\sum_{i=1}^{m} \frac{1}{k} \sum_{j=1}^{k} (u'_i)_j \frac{r_i}{T}}{\sum_{i=1}^{m} \frac{r_i}{T}} \qquad (2)$$

with an estimate of variance

$$s_v^2 = \frac{\sum_{i=1}^{m} \frac{1}{k} \sum_{j=1}^{k} (u'_i - \langle u' \rangle)_j^2 \frac{r_i}{T}}{\sum_{i=1}^{m} \frac{r_i}{T}} \qquad (3)$$

Here k is the number of data points taken at a particular radial position, m is the number of radial positions, and r_i/T is a weighting factor which accounts for the increase of volume with radial position.

EXPERIMENTAL RESULTS

Turbulent Velocities

The axial, radial, and tangential turbulent velocities were measured throughout the volume of the standard tank by varying r, γ, and z. Table 2 gives the space averaged turbulent velocities and estimates of variance in the three directions at four impeller speeds. The rather low variance indicates that the velocities do not differ much from one location to another. The turbulent velocities in the radial and the tangential direction appear somewhat smaller than the turbulent velocities in the axial direction; however, the turbulent velocities in the axial direction are the most reliable. This is because the mean flow in the bulk of the tank is essentially in the axial direction, away from the impeller stream in the region covered by the baffles and towards the impeller in the core of the tank. If the shielded hot-wire probe is inserted through the top of the tank to measure the tangential and radial velocity components, the shield is nearly parallel to the mean velocity vector. Figure 10 of Günkel et al. (1971) shows that under this condition the probe is less reliable.

In Table 3 the local turbulent velocities in the axial direction are shown as a function of the radial coordinate. Also shown are the local mean velocities and the turbulence intensity. The turbulence intensity in the bulk of the tank was of the order of 60%. This is between the turbulence intensity of 75% reported by Levins and Glastonbury (1972) and of 35% reported by Schwartzberg and Treybal (1968) in liquid filled stirred tanks. In Figure 1 the turbulent velocities in the standard tank are shown for several locations as a function of the impeller speed. The turbulent velocities are directly proportional to the impeller rotation rate at rates greater than 8 rev./s. This speed corresponds to an impeller Reynolds number of 1.5×10^4, which is close to the critical Reynolds number obtained from power studies, that is, the Reynolds number above which the power number is constant. The spread of the data shown in Figure 1 is typical of the variation of u' throughout the tank.

Table 3. The Root-Mean-Square Velocities and the Turbulence Intensities in Axial Direction in the Bulk of the Tank

$\gamma = 0$, $z = -12$ cm, $N = 15.8$ s^{-1}

r, cm	$\overline{U}_{ax}$, m/s	u'_{ax}, m/s	$\frac{u'_{ax}\, 100}{U_{ax}}$ %	r, cm	$\overline{U}_{ax}$, m/s	u'_{ax}, m/s	$\frac{u'_{ax}\, 100}{U_{ax}}$ %
0	2.76	1.70	62	12	2.40	1.63	68
1	2.73	1.59	58	13	2.19	1.64	75
2	3.15	1.48	47	14	2.33	1.63	70
3	3.16	1.37	43	15	2.40	1.59	66
4	3.26	1.29	40	16	2.34	1.52	65
5	3.30	1.29	39	17	2.08	1.52	73
6	3.14	1.32	42	18	1.62	1.48	91
7	2.96	1.44	49	19	0.92	1.67	182
8	2.76	1.50	54	20	−1.34	1.81	136
9	2.73	1.52	56	21	−2.51	1.80	72
10	2.43	1.59	65	22	−3.56	1.44	40
11	1.22	1.59	72	22.8	−2.12	0.95	45

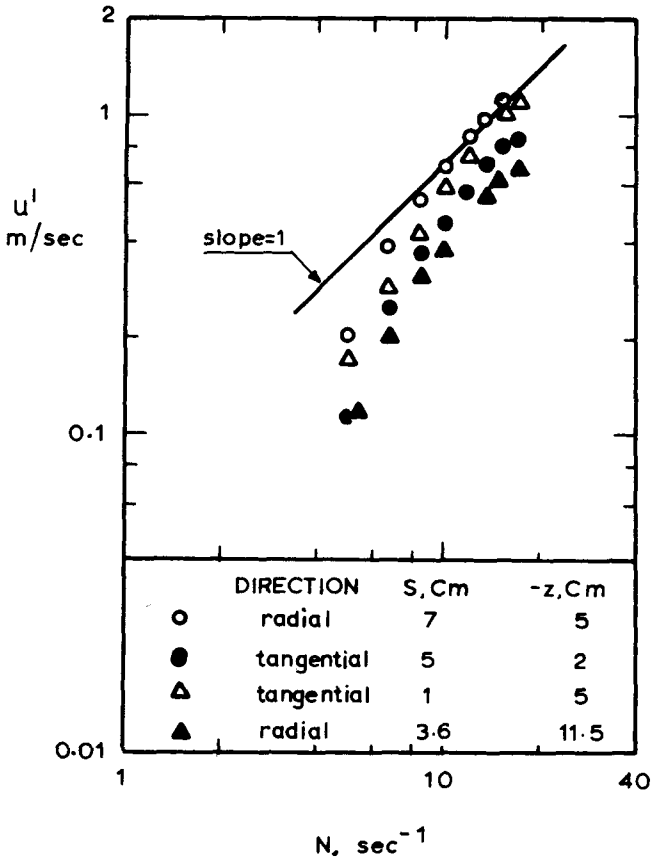

Fig. 1. Root mean square fluctuating velocity in the bulk of the tank.

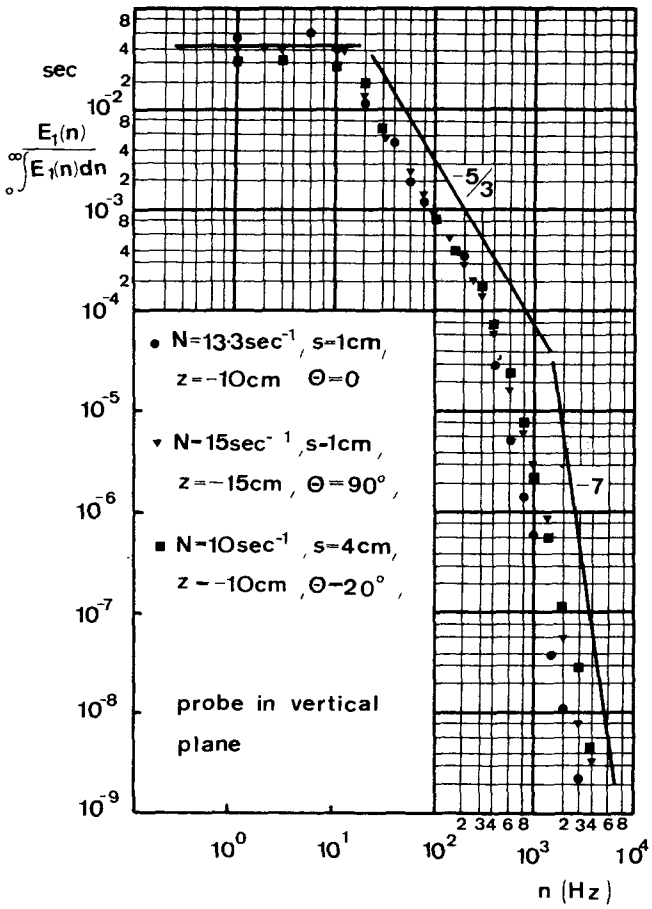

Fig. 2. One-dimensional energy spectra in the bulk of the tank for the standard system.

From the work in the standard tank-impeller system, it was concluded that the axial velocities were measured with the best accuracy and that the spatial variation of turbulent velocity was small. Thus, in the other systems the axial velocities were measured at a smaller number of locations. Typically, data were obtained at a number of radial positions at a single axial location. Equations (2) and (3) were then used to obtain $\langle u' \rangle$ and s_v^2. The measurements are summarized in Table 4. Experiments 5-8 and 9-12 were with the same tank and impeller but at two different axial locations. These data demonstrate that the choice of the axial position hardly affects the measured space average turbulent velocity. In all other experiments the probe was located halfway between the bottom of the tank and the impeller. In all cases the velocity varied so little that the space average value of u'^2 was within 5% of $\langle u' \rangle^2$.

TABLE 4. THE AVERAGE TURBULENT VELOCITIES IN VARIOUS TANK-IMPELLER SYSTEMS

Impeller type	Exp. no.	T, cm	D, cm	w/D	N, s^{-1}	$-z$, cm	$\langle u'_{ax} \rangle$, m/s	$\frac{100\, s_v}{\langle u'_{ax} \rangle}$ %
Six blade	1	45.7	22.8	0.2	6.67	12.0	0.50	22
Disk style	2				10.0		0.90	14
Turbine	3				13.3		1.22	16
Impeller	4				15.8		1.53	14
	5	45.7	22.8	0.4	6.67	7.5	0.64	17
	6				10.0		1.09	20
	7				13.3		1.44	20
	8				15.0		1.66	16
	9	45.7	22.8	0.4	6.67	15.0	0.75	17
	10				10.0		1.21	16
	11				13.3		1.62	17
	12				15.0		1.80	17
	13	91.4	45.7	0.2	3.33	22.5	0.52	12
	14				6.67		1.11	12
	15				10.0		1.57	8
	16	91.4	30.5	0.2	10.0	22.5	0.62	8
	17				13.3		0.86	10
Four blade	18	45.7	22.8	0.2	10.0	12.0	0.77	4
Turbine (No disk)	19				13.3		1.01	4

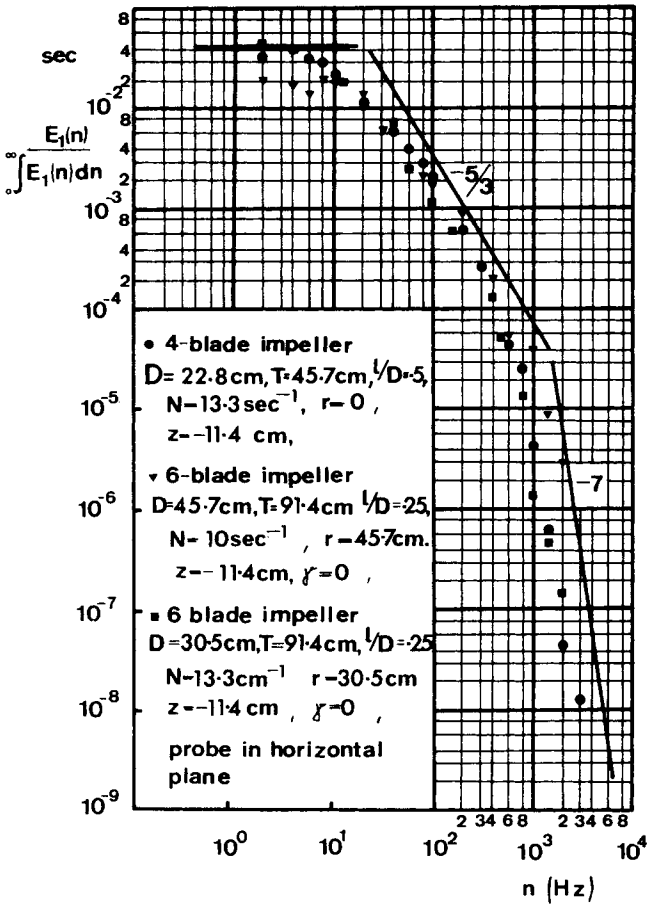

Fig. 3. One-dimensional energy spectra in the bulk of the tank for several tank-impeller systems.

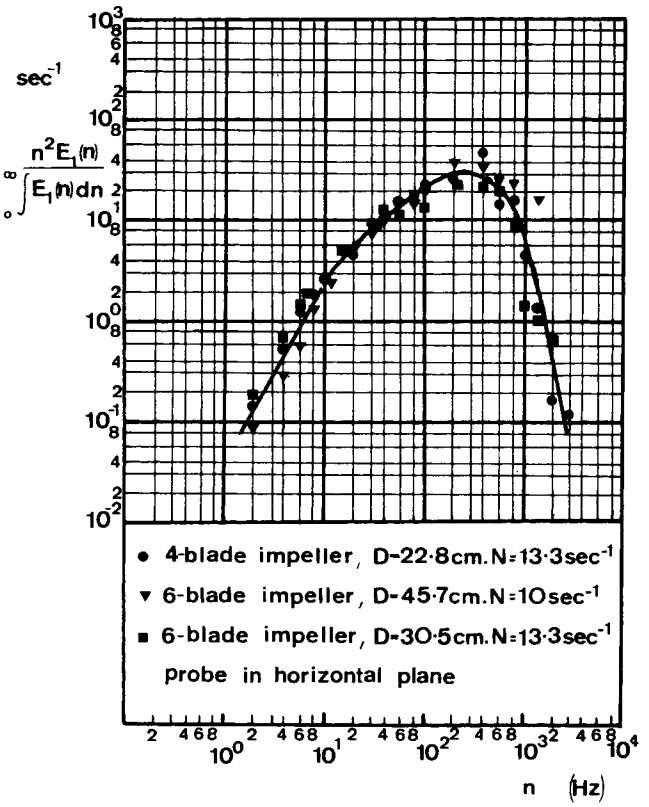

Fig. 4. One-dimensional dissipation function in the bulk of the tank.

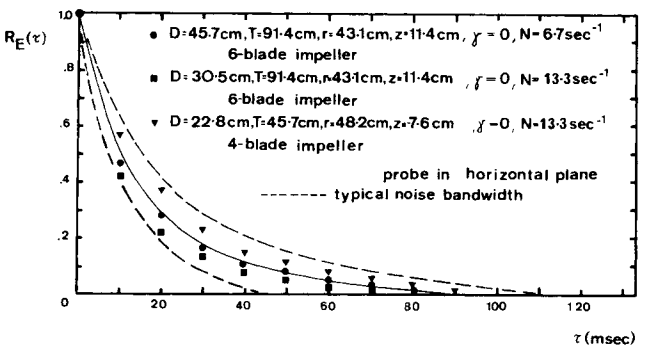

Fig. 5. Eulerian autocorrelation function in the bulk of the tank for several tank-impeller systems.

One-Dimensional Energy Spectra

One-dimensional energy spectra of the turbulent velocities in the axial, the tangential, and the radial direction were measured in both tanks for various operating conditions. Some spectra for the radial component of the velocity taken in the bulk of the standard tank are shown in Figure 2, and some spectra for the axial component of the velocity taken in other tank and impeller systems are shown in Figure 3. By graphically integrating the spectra it was confirmed that

$$\int_0^\infty E_1(n)dn = \overline{u_1^2} \tag{4}$$

The spectra in Figures 2 and 3 are normalized by using the integral in Equation (4). All of the more than fifty spectra obtained in different locations in the two tanks, for different velocity components, that is, for different orientations of the probe, for different impellers, and for different speeds, were very similar with some scatter in the high-frequency range. The spectra show three distinct regions with increasing frequency, one with slope zero, one with slope of about $-5/3$, and one with slope of about -7.

Figure 4 shows the one-dimensional dissipation function computed from

$$\frac{\Phi_1(n)}{\overline{u_1^2}} = \frac{n^2E_1(n)}{\int_0^\infty E_1(n)dn} \tag{5}$$

This form of the dissipation function is obtained if the energy transfer term in the dynamic equation for the energy spectrum is neglected. Most dissipation takes place in the frequency range between 10 and 10^3 Hz. The maximum in the dissipation function is between 100 and 300 Hz.

Eulerian Autocorrelation Function

The Eulerian autocorrelation function

$$R_E(T) = \frac{\overline{u_i(t)u_i(t+\tau)}}{u_i^2(t)} \tag{6}$$

was measured in various sections of the two tanks, for different impellers and operating conditions. The correlograms computed by the PAR signal correlator were plotted on an x-y recorder, graphically interpolated, normalized, and then replotted. All correlograms were taken at least ten times. In Figure 5 the autocorrelation function is shown for a variety of conditions. The noise level, that is, the scattering observed when the correlogram was measured several times at the same location under the same operating conditions, is indicated. All the correlograms obtained for different operating conditions were very similar. The Eulerian integral time scale, which is obtained by integrating the Eulerian autocorrelation function,

Table 5. Correlation of the Turbulence Parameters

Experiment number	P, $\frac{m^2\,kg}{s^3}$	V, m^3	ϵ, $\frac{m^2}{s^3}$	$\langle u' \rangle$, $\frac{m}{s}$	v, $\frac{m}{s}$	η, cm	λ_g, cm	Re_λ	l_e, cm
1	1.12	0.075	12.4	0.50	0.117	0.0130	0.215	72.0	1.52
2	3.77	0.075	42.0	0.90	0.158	0.0095	0.208	124.0	2.61
3	8.94	0.075	99.0	1.22	0.197	0.0077	0.185	149.0	2.76
4	14.95	0.075	165.0	1.53	0.224	0.0068	0.179	181.0	3.27
5	2.24	0.075	24.7	0.64	0.139	0.0109	0.194	82.0	1.59
6	7.54	0.075	83.3	1.09	0.188	0.0080	0.180	130.0	2.32
7	17.87	0.075	197.3	1.44	0.234	0.0065	0.155	148.0	2.28
8	25.30	0.075	280.0	1.66	0.256	0.0059	0.150	165.0	2.45
9	2.24	0.075	24.7	0.75	0.139	0.0109	0.225	112.0	2.56
10	7.54	0.075	83.3	1.21	0.188	0.0080	0.200	160.0	3.18
11	17.87	0.075	197.3	1.62	0.234	0.0065	0.173	186.0	3.08
12	25.30	0.075	280.0	1.80	0.256	0.0059	0.162	193.0	3.12
13	4.46	0.600	6.2	0.52	0.098	0.0154	0.314	108.0	3.40
14	35.80	0.600	49.4	1.11	0.165	0.0092	0.238	175.0	4.13
15	120.90	0.600	166.7	1.57	0.224	0.0067	0.183	190.0	3.48
16	15.87	0.600	22.1	0.62	0.135	0.0112	0.198	81.0	1.62
17	37.60	0.600	51.9	0.86	0.168	0.0090	0.180	102.0	1.85
18	2.48	0.075	27.4	0.77	0.142	0.0106	0.221	113.0	2.48
19	5.89	0.075	65.0	1.01	0.177	0.0085	0.189	126.0	2.38

Average value of l_e = 2.64 cm
Standard deviation = 0.69 cm

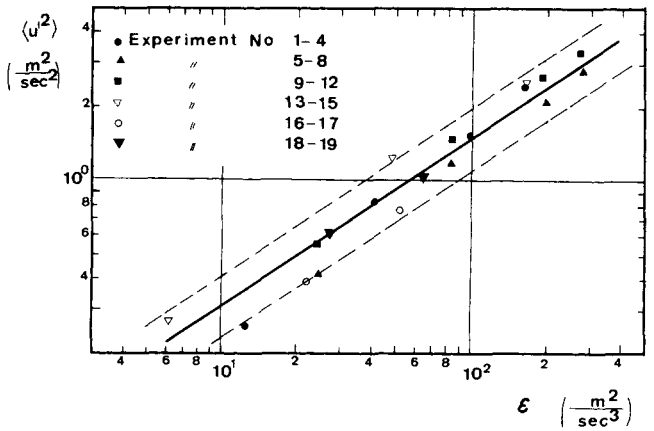

Fig. 6. Mean square fluctuating velocity in the bulk of the tank as a function of power input.

differed in the extreme case by a factor 3. The Eulerian integral time scales for the radial and the tangential velocity components were somewhat smaller than the scale for the axial component. It is again thought that the relatively poorer accuracy of the shielded hot-wire probe when placed parallel to the mean flow direction is responsible for this result.

DISCUSSION

Treatment of the data is based upon the assumption that the turbulence in the bulk of the tank is isotropic. This assumption is supported by the small variation in the root-mean-square value of the fluctuating velocity throughout the bulk of the tank, the essentially similar spectra of the radial, axial and tangential components of the velocity throughout the bulk of the tank, and the existence of a $-5/3$ range in all of the measured energy spectra. Without this assumption, no further treatment of the experimental data would be possible. However, one must keep in mind that the condition of local isotropy is only a model which is approximated to some extent in flows having large turbulence Reynolds numbers.

The Turbulent Velocities

Assuming, then, that the energy transmitted into the tank is dissipated in the bulk of the tank through the turbulent motion and that the turbulence is isotropic and homogeneous, we can simplify the turbulent energy equation to

$$\frac{P}{\rho V} \equiv \epsilon = 15\nu \frac{\langle u'^2 \rangle}{\lambda_g^2} \tag{7}$$

where λ_g is the lateral Eulerian microscale.

In Figure 6 the measured values of $\langle u'^2 \rangle$ are plotted on a logarithmic scale against the energy dissipation per unit mass. The latter quantity was calculated from the power numbers presented in Table 1. All the data fall close to a line with slope 2/3:

$$\langle u'^2 \rangle \alpha \epsilon^{2/3} \tag{8}$$

The dotted lines in Figure 6 represent the error of $\pm 15\%$ in the velocity measurements. As a consequence of the correlation of Figure 6 and Equation (7)

$$\lambda_g^2 \alpha \epsilon^{-1/3} \tag{9}$$

The turbulence Reynolds number obtained by combining this microscale and the turbulent velocity is calculated from

$$Re_\lambda = \frac{\langle u' \rangle \lambda_g}{\nu} \tag{10}$$

The length and velocity scale of the Kolmogoroff equilibrium range were calculated from

$$v = (\nu\epsilon)^{1/4} \tag{11}$$

$$\eta = (\nu^3/\epsilon)^{1/4} \tag{12}$$

Table 5 summarizes the results for each experiment listed in Table 4. For the range of operating conditions covered in this study, the turbulence Reynolds number Re_λ was between 72 and 193. For values of Re_λ in this range, a $-5/3$ inertial subrange appears, and local isotropy is a fair approximation for grid generated turbulence but not for turbulent shear flow where higher Re_λ is required

(Brodkey, 1967).

Rearranging Equation (8), we get

$$\epsilon \alpha \langle u'^3 \rangle \tag{13}$$

This last equation is of the same form as a semiempirical equation proposed by Batchelor (1953)

$$\epsilon = \frac{3}{2} A \frac{\langle u'^3 \rangle}{l_e} \tag{14}$$

where l_e is the scale of the energy containing eddies, and A is a numerical constant which was found from wind tunnel experiments to be near unity. In all subsequent calculations, A was taken to be 1. The scale of the energy containing eddies l_e computed from Equation (14) is shown in Table 5. The data are scattered around an average value of 2.6 cm. The scales for the large and small tanks were not statistically different: $l_e = 2.90$ cm with $s_v = 0.98$ cm in the large tank and $l_e = 2.54$ cm with $s_v = 0.52$ cm in the small tank. The range of scales computed for different tanks, for different impellers, and for different impeller speeds is small considering that these scales were computed from velocity data raised to the power 3.

The observation that the scale of the energy containing eddies remains constant for the experimental conditions covered in this study is rather surprising. It is generally thought that the scale of the largest eddies is related to the dimensions of the flow system and in particular that the scale of the energy containing eddies is of the same order of magnitude as the scale of the obstruction responsible for generating the turbulence. Figure 3 in Part I shows that the flow in the bulk of the tank is towards the impeller; thus it is difficult to see how the scale of the turbulent eddies generated by the impeller can be preserved after the interaction of the impeller stream with the fluid entrained from the bulk of the tank and with the baffles. As Figure 9 of Part I shows, the periodic velocity fluctuations have disappeared before the impeller stream reaches the wall; hence, all information about the shape of the impeller has been lost before the wall is reached. It is not yet clear which factors determine the size of the energy containing eddies in the bulk of the tank; however, the scale of these eddies is much smaller than the tank diameter.

Equation (14) may be rewritten to show the dependence of $\langle u' \rangle$ upon ϵ explicitly:

$$\langle u' \rangle = (2/3)^{1/3} \epsilon^{1/3} l_e^{1/3} \tag{15}$$

This may be compared to Equation (1) which can be rewritten as follows:

$$u' = 0.73 \left(\frac{\pi}{4N_p} \right)^{1/3} \epsilon^{1/3} D^{1/3} \tag{16}$$

The similarity of the equations is obvious. Schwartzberg and Treybal's expression, Equation (16), shows only a weak effect of the size of the tank-impeller system through the $D^{1/3}$ term.

If it is recalled that in this study the tank diameter was varied by a factor 2, that the turbine impellers of different design were used, that the impeller blade width was varied by a factor 2, that the power input was varied by a factor 40, and that the impeller speed was varied over a wide range, the correlation of all the data with Equations (7) and (14) is striking. This gives confidence in the soundness of the assumptions that the energy transmitted into the tank is dissipated outside the impeller stream through the turbulent motion and that the turbulence in the bulk of the tank is approximately homogeneous and isotropic.

The Integral Scale of Turbulence

The Eulerian integral time scale is obtained by integrating the Eulerian autocorrelation function

$$T_E = \int_0^\infty R_E(t)\,dt \tag{17}$$

From an integration of Figure 5, the value of 19 ms is obtained. An inspection of the more than 100 correlograms taken in this study showed that the Eulerian integral time scale did not change significantly over the range of operating conditions covered. The spread in the scales obtained was similar to the spread obtained for the scale of the energy containing eddies. No systematic relation between the tank and the impeller geometry and the integral time scale was found.

Hinze (1959), assuming a von Karman interpolation for the energy spectrum, obtained

$$L_f = 0.75 l_e \tag{18}$$

Use of the average value of $l_e = 2.6$ cm gives the following estimate of the integral scale of turbulence in the bulk of a stirred tank:

$$L_f = 1.95 \text{ cm} \tag{19}$$

A combination of this scale with the Eulerian integral time scale permits the computation of the apparent convection velocity of the turbulent flow field:

$$L_f = U_c T_E \tag{20}$$

Hence

$$U_c = 1.03 \text{ m/s} \tag{21}$$

The significance of this velocity is not known; however, it is of the same order of magnitude as the turbulent velocities in the bulk of the stirred tank but smaller than the mean velocity.

Transformation of the Spectra into the Wave Number Space

The spectra presented in Figures 2 and 3 are in the frequency space. If these spectra could be transformed into the wave number space, the major result of Part I could be checked, since the energy dissipation in the bulk of the tank could then be calculated from

$$\epsilon = 15\nu \int_0^\infty k^2 E_1(k)\,dk \tag{22}$$

where $E_1(k)$ is the one-dimensional energy spectrum in the wave number space. In the bulk of the tank the turbulence intensity is so high that Taylor's hypothesis cannot be used to transform frequency into wave number. An alternative transformation is proposed here based on two assumptions.

The first assumption is that the shape of the spectrum in the wave number space is the same as the shape of the spectrum in the frequency space. The spectrum in the wave number space will have a range where the slope is equal to zero, followed by a range of about 1.5 decades where the slope is close to $-5/3$. It is expected that the transition point between these two ranges will be close to the wave number corresponding to the size of the energy containing eddies. In the high wave number region there will be a range where the slope of the energy spectrum is close to -7. This range starts near the wave number corresponding to the size of the smallest eddies present in the flow field. The second assumption is that the spectrum in the wave number space can be fitted by a mathematical expression of the following form

$$E_1(k) = \frac{B}{(1 + l_e k)^{5/3} (1 + \eta k)^7} \tag{23}$$

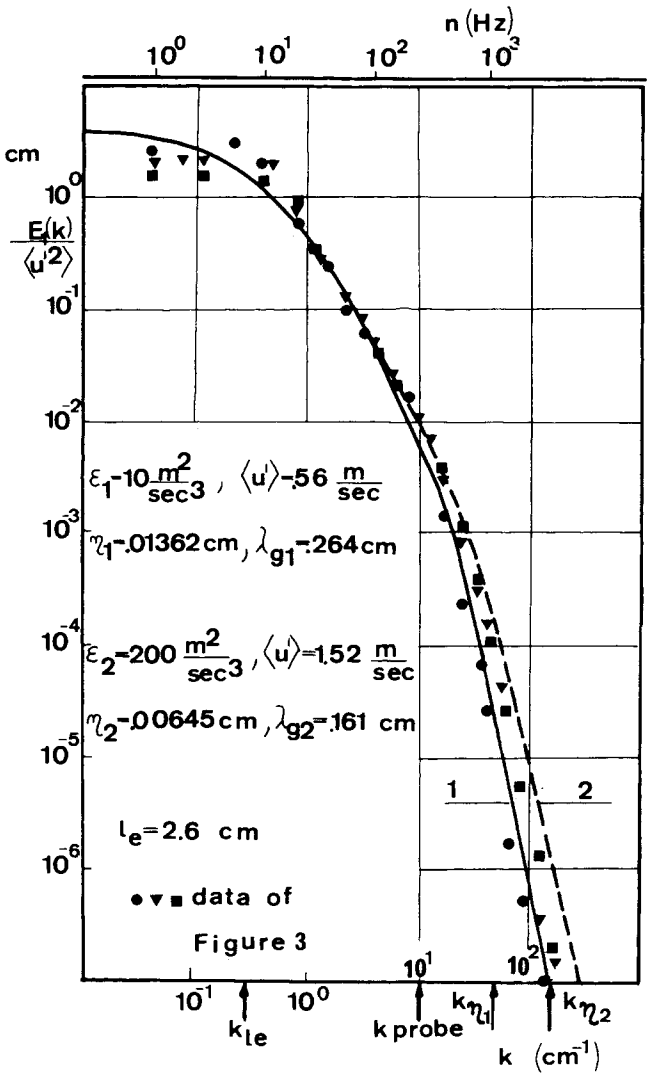

Fig. 7. One-dimensional energy spectrum in the bulk of the tank as a function of wavenumber.

where B is a constant. The form of Equation (23) was chosen, in part, because it is similar to expressions giving the mathematical representation of Bode diagrams. Bode diagrams are like energy spectra in that they show distinct ranges having constant slopes with smooth transitions between these ranges. Additional justification for the form of Equation (23) is given subsequently.

The turbulent velocity is related to the energy spectrum by

$$\langle u'^2\rangle = \int_o^\infty E_1(k)\,dk \tag{24}$$

The constant B in Equation (23) can be estimated by noting that most of the energy is concentrated in the low wave number region and that in this region the energy spectrum is well approximated by using only the first term in the denominator of Equation (23):

$$B = \langle u'^2\rangle \Big/ \int_o^\infty \frac{dk}{(1 + l_e k)^{5/3}} \tag{25}$$

Integration yields

$$B = \frac{2}{3} l_e \langle u'^2\rangle \tag{26}$$

The one-dimensional energy spectrum in the wave number space becomes

$$\frac{E_1(k)}{\langle u'^2\rangle} = \frac{2l_e/3}{(1 + l_e k)^{5/3}\,(1 + \eta k)^7} \tag{27}$$

Figure 7 shows the spectra from Figure 2 plotted in the wave number space. The lines were obtained from Equation (27) with l_e = 2.6 cm and η, the scale of the smallest energy containing eddies, taking its extreme values: 0.00645 and 0.0136 cm. Equation (27) is in good agreement with the experimental findings in that the energy spectra are very similar over the whole range of operating conditions. Only in the high wave number region, and this is the region where the experimental data show some scatter, does Equation (27) discriminate between spectra for low power inputs and spectra for high power inputs. The curves of Figure 7 provide an excellent fit to the experimental spectra shown in Figures 2 and 3. By comparing the scales at the top and the bottom of Figure 7 a relation between the frequency and the wave number can be obtained; a frequency of 1 Hz corresponding to a wave number of 4×10^{-2} cm^{-1}. The apparent convection velocity of the turbulent flow field is therefore

$$U_c = \frac{2\pi n}{k} = 1.57 \text{ m/s} \tag{28}$$

This velocity is slightly higher than the convection velocity computed in Equation (21); however, it is still in the range of the turbulent velocities measured in this study.

Also indicated on Figure 7 are the wave numbers corresponding to the size of the energy containing eddies l_e, the smallest eddies η, and the probe. The wave numbers were obtained by taking the reciprocals of l_e, η, and the diameter of the hole in the probe shield. Despite the fact that $Re_\lambda < 200$, the data show a good separation between k_{l_e} and k_η as required for the existence of a $-5/3$ inertial subrange. The experimental data for wave numbers much larger than k_{probe} are suspect.

Mujumdar et al. (1970) computed the longitudinal integral length scale from

$$L_f = \frac{U_c E_1(0)}{4u'^2} \tag{29}$$

The conditions for applying this relation are discussed by Hinze (1959). Reading from Figure 2 for the value of the zero intercept a value of 4.5×10^{-2} s and using the apparent convection velocity of the turbulent flow field given by Equation (28), we get for L_f

$$L_f = 1.77 \text{ cm} \tag{30}$$

This value of L_f is very close to the value obtained earlier in Equation (19).

In Figure 8 the dissipation spectra of Figure 4 are replotted in the wave number space. The curves obtained by using Equation (27) for the energy spectrum give a good fit to the data up to frequencies of 10^3 Hz, where most of the dissipation takes place. However, the decrease of the spectrum in the high-frequency region seems to be sharper than predicted. This could mean that the exponent in the second term in the denominator of Equation (27) should be larger; however, as noted above, the data in this region cannot be considered reliable. At the moment the slope of the spectrum in the high wave number range is unknown, although a slope of -7 has been predicted by Heisenberg (1948).

Further justification for the form of the spectrum chosen here, Equation (27), comes from a comparison with the results of Grant et al. (1962). In the inertial range where $E_1(k)$ is proportional to $k^{-5/3}$, the one-dimensional spectrum can be approximated by

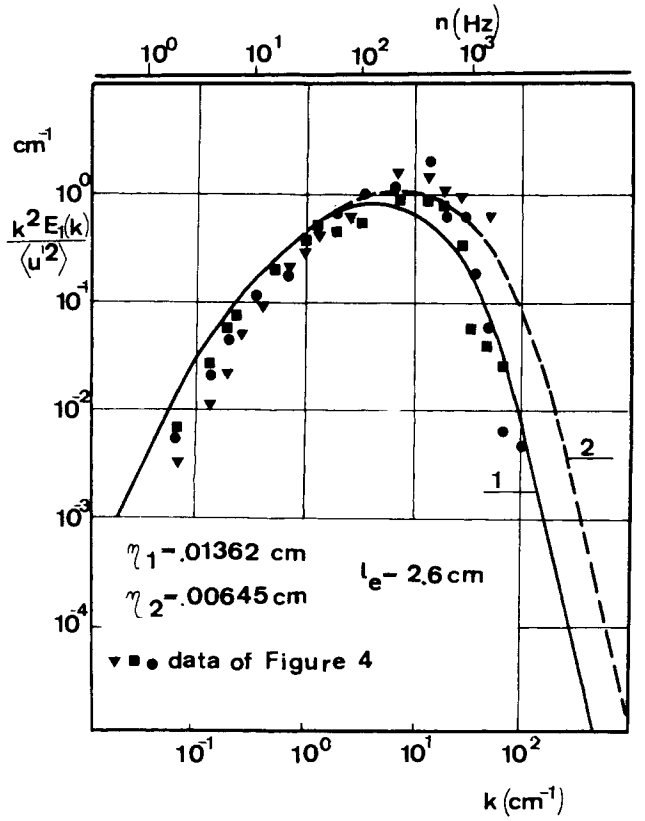

Fig. 8. One-dimensional dissipation spectrum in the bulk of the tank as a function of wavenumber.

$$E_1(k) = C\epsilon^{2/3}/k^{5/3} \tag{31}$$

Grant et al. determined the constant C from measurements on a turbulent flow with a very large value of Re_λ. Their data gave

$$C = 0.47 \pm 0.02 \tag{32}$$

Equation (27) evaluated for the same range yields

$$E_1(k) = 2\langle u'^2\rangle/3l_e^{2/3}\,k^{5/3} \tag{33}$$

Combining Equation (15) with Equation (33), we get

$$E_1(k) = \left(\frac{2}{3}\right)^{5/3} \epsilon^{2/3}/k^{5/3} \tag{34}$$

Thus, Equation (27) provides an estimate for C of $(2/3)^{5/3} = 0.509$, which is in good agreement with the data of Grant et al. (1962) summarized in Equation (32).

With the transformation to the wave number space now complete, the energy dissipated in the bulk of the tank can be estimated through Equation (22). By using the extreme operating conditions of this study, $\eta = 0.00645$ cm and $\eta = 0.01362$ cm, Equation (22) was integrated numerically to give the results shown in Table 6. The rate of energy dissipation computed from Equation (22) is approximately 62% of the energy input calculated through the power number correlations. Since the data were space averaged and the transformation to the wave number space was not certain, the agreement between the two values of ϵ is considered excellent. This is a good check on the conclusion of Part I that essentially all of the energy put into the tank is dissipated in the bulk of the tank through the turbulent motion.

Table 6. Comparison of Energy Dissipation Calculated from N_p and from the Integration of Equation (22)

ϵ, m^2/s^3 from power correlation	η, cm	l_e, cm	$\langle u'\rangle$, m/s	ϵ, m^2/s^3 from Equation (24)
10	0.00645	2.6	0.56	6.1
200	0.01362	2.6	1.52	126

Extension of the Results to Liquid Systems

Equations (7) and (14) will apply to stirred tanks containing low viscosity liquids. In the turbulent range, the power input per unit mass can be computed from a power correlation:

$$\epsilon = \frac{4N_pN^3D^5}{\pi T^2H} \tag{35}$$

Hence, there are three equations, (7), (14), and (35), with four unknowns, $\langle u'\rangle$, λ_g, ϵ, and l_e. In the following some evidence is presented which supports the postulate that the scale l_e will be approximately the same in air and in water.

In the low wave number range, where most of the turbulence energy is concentrated, the energy spectrum has a slope of $-5/3$. The same was observed in liquid systems by Kim and Manning (1964), by Rao and Brodkey (1972), by Sato et al. (1967), and by Cho et al. (1971). Concentration spectra measured by Manning and Wilhelm (1963), by Reith (1965), and by Cho et al. (1971) also show a range with slope $-5/3$. Kolmogoroff (see Hinze, 1959) predicted such a slope for an inertial subrange of the universal equilibrium range where viscosity effects play no role; thus the presence of a range where the energy spectrum has a slope of $-5/3$ implies that the turbulence in this range is not a function of the viscosity. As a consequence, the turbulent velocity and the scale most characteristic of this inertial range, that is, $\langle u'\rangle$ and l_e, are not affected by the viscosity and are the same in air and liquids of low viscosity. There is some experimental evidence to support this speculation. The longitudinal integral length scale reported in the literature for liquid-stirred tanks is typically $L_f \sim 1$ cm. Outside the impeller stream Cutter (1966) found values for L_f between 0.49 and 0.99 cm. In the impeller stream Rao and Brodkey (1972) found $L_f = 0.475$ cm, while Cho et al. (1971) found values between $L_f = 0.19$ cm and $L_f = 1.2$ cm. These scales are of the same magnitude as $L_f = 1.95$ cm and $L_f = 1.77$ cm obtained through two different methods in this study. Clearly, L_f and also l_e are of the same order of magnitude for low viscosity liquids and for air. Even if there is some difference, the turbulent velocity $\langle u'\rangle$ computed from Equation (14) would not be affected very much because the exponent over $\langle u'\rangle$ is 3.

Based on these arguments, it is assumed that the present results can be extended to liquid systems by assuming that $l_e = 2.6$ cm. Now $\langle u'\rangle$ can be computed from Equation (5), and λ_g can be computed from Equation (7). This procedure is valid only if Re_λ is large enough, that is, $Re_\lambda > 100$. This critical Reynolds number corresponds to starting the fully turbulent range at $N \sim 8$ s^{-1} in the standard system used in this study (see Figure 1). It should be noted that above procedure implies that the turbulent motion in the bulk of two different stirred tanks is the same at equal power input per unit mass, even if the impeller Reynolds numbers and the geometry are not the same. In the following section one application of the present results is given.

Mass Transfer from Suspended Particles

Mass transfer from a single sphere to a fluid flowing past it can be described by an equation of the following

form

$$Sh_p = 2 + bRe_p^a\, Sc^{1/3} \tag{36}$$

where $a = 1/3$ for $Re_p < 1$ and a $1/2$ for $Re_p > 10$. A review of published experimental work on mass transfer from suspended particles is presented by Günkel (1973). It is sufficient here to note that over a wide range of sizes for fairly large particles, the mass transfer coefficient is not a function of the particle diameter (Furusawa and Smith, 1973; Barker and Treybal, 1960; Humphrey and van Ness, 1957), while for very small particles the mass transfer coefficient increases with decreasing particle diameter (Harriot, 1962; Brian et al., 1969; and Levins and Glastonbury, 1972).

Levins and Glastonbury (1972) found that particles suspended in a stirred tank followed the path of the large turbulent eddies and that slip between the particles and the fluid was small. Therefore, it is the small eddies of approximately the same size as the suspended particles which are responsible for the mass transfer, and the Reynolds number in Equation (36) should be written

$$Re_p = \frac{u_k d_p}{\nu} \tag{37}$$

where u_k is the velocity of the eddies in the wave number range corresponding to the size of the particles. It was found in the present study that

$$<u'> \alpha\ (l_e\epsilon)^{1/3} \tag{38}$$

It was also found that the energy spectra were about the same for all operating conditions and that the energy spectra in the inertial range were proportional to $k^{-5/3}$. Hence

$$u_k \alpha\ (l_e\epsilon)^{1/3}\ (l_e k)^{-5/6} \tag{39}$$

Replacing the wave number by the reciprocal of the particle diameter, we get

$$u_k \alpha\ (l_e\epsilon)^{1/3}\ (d_p/l_e)^{5/6} \tag{40}$$

and finally

$$Re_p \alpha\ \epsilon^{1/3}\, d_p^{11/6}/l_e^{1/2}\nu \tag{41}$$

We also note that impeller and tank variables can be used in place of ϵ through Equation (35):

$$Re_p \alpha\ ND^{4/3}\ (D/T^2H)^{1/3}\, d_p^{11/6}/l_e^{1/2}\nu \tag{42}$$

Substitution of Equation (41) or (42) into Equation (36) yields a predicted form for the Sherwood number. For example, for large Re_p, $Sh >> 2$, and

$$Sh_p \alpha\ \frac{\epsilon^{1/6} d_p^{11/12}}{l_e^{1/4}\,\nu^{1/2}}\ Sc^{1/3} \tag{43}$$

or

$$Sh_p \alpha\ \frac{N^{1/2}D^{2/3}d_p^{11/12}}{l_e^{1/4}\,\nu^{1/2}} \left(\frac{D}{T^2H}\right)^{1/6} Sc^{1/3} \tag{44}$$

In each case the mass transfer coefficient is only weakly dependent on particle diameter. Correlations similar to Equations (43) and (44) have been proposed (see Brian et al., 1969; Levins and Glastonbury, 1972; and Miller, 1971).

ACKNOWLEDGMENT

This work was supported by a grant from the National Research Foundation of Canada. One of us (A.G.) was supported by a fellowship from the McConnell Foundation.

NOTATION

A, B, C = constants
a, b = constants
D = impeller diameter
d_p = particle diameter
$E_1(k)$ = one-dimensional energy spectrum in the wave number space
$E_1(n)$ = one-dimensional energy spectrum in the frequency space
H = height of tank
k = wave number
L_f = longitudinal integral length scale
L_L = Lagrangian integral length scale
l = length of impeller blades
l_e = scale of energy containing eddies
N = rate of rotation of impeller
N_p = power number $= P/\rho N^3 D^5$
n = frequency
P = power input
R_E = Eulerian autocorrelation function
Re_p = particle Reynolds number
Re_λ = turbulence Reynolds number
r = radial coordinate
s_v^2 = estimate of variance
Sc = Schmidt number
Sh_p = particle Sherwood number
T = tank diameter
T_E = Eulerian integral time scale
t = time
U_c = apparent convection velocity
$\overline{U}$ = mean velocity
u = fluctuating velocity
u' = root-mean-square value of the fluctuating velocity
$<u'>$ = space averaged value of u'
V = volume of tank
u = Kolmogoroff velocity scale
w = impeller blade width
z = axial coordinate

Greek Letters

ϵ = rate of energy dissipation per unit mass
λ_g = lateral Eulerian microscale
ν = fluid kinematic viscosity
$\Phi_1(n)$ = one-dimensional dissipation spectrum in the frequency space
ρ = fluid density
τ = time delay in autocorrelation function
η = Kolmogoroff length scale
γ = angle measured in horizontal plane from baffle

Subscripts

ax = axial
rad = radial
tan = tangential

LITERATURE CITED

Barker, J. J., and R. E. Treybal, "Mass Transfer Coefficients for Solids Suspended in Agitated Liquids," *AIChE J.*, **6**, 289 (1960).

Batchelor, G. K., *The Theory of Homogeneous Turbulence*, Cambridge University Press, London (1953).

Bates, R. L., P. L. Fondy, and R. R. Corpstein, "Examination of Some Geometric Parameters of Impeller Power," *Ind. Eng. Chem. Proc. Design Develop.*, **2**, 310 (1963).

Brian, P. L. T., H. B. Hales, and T. K. Sherwood, "Transport of Heat and Mass Between Liquids and Spherical Particles in an Agitated Tank", *AIChE J*, **15**, 727 (1969).

Brodkey, R. S., *The Phenomena of Fluid Motions*, Chapt. 14, Addison-Wesley, Reading, Mass. (1967).

Cho, S. H., P. H. Amarnath, and H. A. Becker, "Turbulence and Mixing in a Stirred Tank," paper presented at the 21st Canadian Chemical Engineering Conference, Montreal, Canada (Oct., 1971).

Cutter, L. A., "Flow and Turbulence in a Stirred Tank,"

AIChE J, 12, 35 (1966).
Furusawa, T., and J. M. Smith, "Fluid-Particle and Intraparticle Mass Transport Rates in Slurries," *Ind. Eng. Chem. Fundamentals*, 12, 197 (1973).
Grant, H. L., R. W. Stewart, and A. Moilliet, "Turbulence Spectra from a Tidal Channel," *J. Fluid Mech.*, 12, 241 (1962).
Günkel, A. A., "Flow Phenomena in Stirred Tanks", Ph.D. thesis, McGill University, Montreal, Canada (1973).
———., R. P. Patel, and M. E. Weber, "A Shielded Hot-Wire Probe for Highly Turbulent Flows and Rapidly Reversing Flows," *Ind. Eng. Chem. Fundamentals*, 10, 627 (1971).
Harriott, Peter, "Mass Transfer to Suspended Particles: Part I. Suspended in Agitated Tanks," *AIChE J.*, 8, 93 (1962).
Hinze, J. O., *Turbulence*, McGraw-Hill, New York (1959).
Humphrey, D. W., and H. C. van Ness, "Mass Transfer in a Continuous Flow Mixing Vessel," *AIChE J.*, 3, 283 (1957).
Kim, W. J., and F. S. Manning, "Turbulence Energy and Intensity Spectra in a Baffled Stirred Tank," *AIChE J.*, 10, 747 (1964).
Levins, D. M., and J. R. Glastonbury, "Particle—Liquid Hydrodynamics and Mass Transfer in a Stirred Vessel; Part I—Particle—Liquid Motion," *Trans. Inst. Chem. Engrs.*, 50, 32 (1972); "Part II—Mass Transfer," *ibid.*, 132.
Manning, F. S., and R. H. Wilhelm, "Concentration Fluctuations in a Stirred, Baffled Vessel," *AIChE J.*, 9, 12 (1963).
Miller, D. N., "Scale-up of Agitated Vessels," *Ind. Eng. Chem. Proc. Design Develop.*, 10, 365 (1971).
Mujumdar, A. S., B. Huang, D. Wolf, M. E. Weber, and W. J. M. Douglas, "Turbulence Parameters in a Stirred Tank," *Can. J. Chem. Eng.*, 48, 475 (1970).
O'Connell, F. P., and D. E. Mack, "Simple Turbines in Fully Baffled Tanks—Power Characteristics," *Chem. Eng. Progr.*, 46, 358 (1950).
Rao, A. M., and R. S. Brodkey, "Continuous Flow Stirred Tank Turbulence Parameters in the Impeller Stream," *Chem. Eng. Sci.*, 27, 137 (1972).
Reith, I. T., "Generation and Decay of Concentration Fluctuations in a Stirred, Baffled Vessel," *AIChE Symposium Series No. 10*, 14 (1965).
Sato, Y., Y. Horie, M. Kamiwano, and K. Yamamoto, "Turbulence Flow in a Stirred Vessel," *Kagaku Kogaku*, 31, 79 (1967).
Schwartzberg, H. G., and R. E. Treybal, "Particle and Fluid Motion in Turbulent Stirred Tanks—Fluid Motion", *Ind. Eng. Chem. Fundamentals*, 7, 1 (1968).
Uhl, V. W., and J. B. Gray, ed., *Mixing—Theory and Practice*, Vol. 1, Academic Press, New York (1966).

Manuscript received June 10, 1974; revision received and accepted April 30, 1975.

Mixing in the Interaction Zone of Two Free Jets

Mixing in the interaction zone of two round free jets with nozzle axes intersecting at half-angles of 15, 30, and 45 deg. has been studied by the smoke scattered light technique. The fields of mean concentration and concentration fluctuation intensity were mapped with one jet marked with smoke, the other jet marked, and both jets marked. The correlation function between the concentration fluctuations associated with fluid of the two nozzle streams has been calculated from the results and is an important characteristic of the mixing field and a significant measure of molecular mixedness. A transport equation for the associated covariance function is derived, and the special features of the mathematical modeling problem for this class of mixing process are discussed. The implications of the results for processes involving chemical reactions are examined.

H. A. BECKER and B. D. BOOTH

Department of Chemical Engineering
Queen's University
Kingston, Ontario, Canada

SCOPE

Rapid and thorough mixing of fluid streams is often accomplished by means of turbulent jets. The mixing may be accomplished by chemical reaction, as in combustion systems where some or all of the jets may take the form of turbulent diffusion flames. In either case, with or without chemical reaction, knowledge of the turbulent mixing process is essential to an understanding of the system performance. The present work is a contribution towards such knowledge in two areas of higher complexity on which published data are meager: mixing fields entered by three or more feed streams and mixing fields with a strongly three-dimensional character. Experimental results are reported for a typical and practically significant example. A theoretical analysis of the special features of the three-stream problem is given and is applied to interpret the experimental data.

The situation chosen for experimental study is that of two jets (both air) issuing into a virtually infinite, stagnant body of fluid (room air). The nozzle axes are coplanar and intersect in the downstream direction; that is, the jets are obliquely aimed towards each other. The angle 2α between the axes was given values of 30, 60, and 90 deg. Interest was focused on the interaction zone where the jets merge and the nozzle fluid from each becomes thoroughly mixed with that of the other. A light-scatter technique was used to study the mixing process. First one nozzle stream was marked with smoke, then the other, and finally both. Measurements were made of the mean (time-average) smoke concentration field and of the root-mean-square value, called the *intensity*, of the turbulent con-

Correspondence concerning this paper should be addressed to H. A. Becker. B. D. Booth is with the Department of Consumer and Corporate Affairs, Government of Canada, Ottawa, Canada.